Computational Insights into the Membrane Fusion Mechanism of SARS-CoV-2 at the Cellular Level

Jimin Wang[1,*], Federica Maschietto[2], Matthew J. Guberman-Pfeffer[2], Krystle Reiss[2], Brandon Allen[2], Yong Xiong[1], Elias Lolis[3], Victor S. Batista[2,*]

Online supporting materials (4 supporting text sections, 4 supporting figures, 3 supporting video sets of 8 video parts, and 24 additional references)

Supporting text

S1. Three conformations of the coronavirus spike protein in the prefusion state

The S protein of SARS-CoV-2 forms a stable trimer (Fig. S1). The S protomer in the pre-fusion state resembles an open right hand in which the 'fingers' correspond to the RBD (Receptor-Binding-Domain) and the SD1 while the 'thumb' corresponds to the NTD of S1 where NTD is the N-terminal domain, SD1 and SD2 denote S1 subdomain 1 and 2, respectively (Fig. S1e, S1f). Within each S protomer, NTD (N-Terminal Domain) of S1 and RBD are separated by > 30 Å (Fig. S1e, S1f). Within the symmetric S trimer, the RBD of one subunit interacts with the NTD of another. These interactions are approximately maintained in the asymmetric open-1 and open-2 conformations, indicating that the motion of the RBD is restrained by its plastic interactions with the NTD of its neighbor within the S trimer (Fig. S1). While the NTDs do not interact with each other within the S trimer, the RBDs interact with each other in the closed conformation, forming a closed central pore with its RBD in a "down" position. In the asymmetric conformations corresponding to open-1 and open-2, two RBDs remain in the "down" position, while one RBD adopts an "up" configuration with different degrees of pore openness. Since two RBDs are in the "down" configuration, they obstruct the central pore for extension of the S2 central stalk. The SD1/SD2 form a trimer with an open central pore, and their positions remain largely unchanged in all three conformations.

The superposition of the open-1 conformation (6vyb) with the closed conformation (6vxx) of the SARS-CoV-2 S monomer within the S trimer shows that its RBDs are in different locations but the remaining structures are nearly identical (Fig. S1g) (20). The superposition of the open-2 conformation of SARS-CoV-1 (6crz) with a closed conformation of SARS-CoV-2 (6vxx) shows similar results aside from sequence variations between SARS-CoV-1 and SARS-CoV-2 (Fig. S1h) (20, 65). Further opening of open-2, relative to open-1, is approximately on the same trajectory. The closed-to-open-1 motion involves a 64.5° rotation with a skew translation of ~2 Å, which moves mainly downward to the viral membrane, bringing the host cellular membrane closer to the viral membrane. The open-1-to-open-2 motion involves rotation by 16.7° with another skew translation of ~2 Å, which again moves downward. The first rotation axis is tilted against the 3-fold axis by 24.1 Å, and the second rotation axis is tilted by 58.2°. The two axes are offset by ~46.6° and by ~10 Å. As a consequence, the closed-to-open-2 motion involves rotation by 76.8°, which is smaller than the expected sum of two individual rotations (82.2°). The second rotation of the RBD is accompanied by a small rotation (less than 5°) of the NTD of the neighboring subunit, so their interactions are largely maintained within the S trimer. The second rotation axis is located inside the NTD of its neighboring subunit, rotating together to some extent. A third open conformation and relationship with the two open conformations in SARS-CoV-1 S protein have already been described (23).

S2. Geometric principles from prefusion to post-fusion states of S trimers

The overall dimension of the S2 central stalk has been established for both pre-fusion and post-fusion states of SARS-CoV-2, SARS-CoV-1, MHV, and other related coronaviruses (Fig. S2) (10, 36, 59, 66). Yet, the structures of three other fusion intermediates remain elusive. For the extended intermediate, the length of the S central stalk would be longer than both the collapsed and hemi-fusion intermediates, which would be similar to the post-fusion structure. A major difference between these elusive fusion intermediate states and the post-fusion state is migration of other structural elements surrounding the central stalk, namely FP from one end to the opposite end so that two membranes are brought together for merging.

We initially compared the pre-fusion and post-fusion structures of the MHV S trimer (Fig. S2), and our results have now been fully confirmed in the cryo-EM structures of SARS-CoV-2 S2 trimers (22, 36, 59). This provides general valuable information about elusive fusion intermediates. The structural quality of both MHV and SARS-CoV-2 S2 trimers remains limited and many important residues in this structure remain unresolved. Both structures displayed strong streaky ESP features perpendicular to the 3-fold axis. The central stalk of MHV S protein (3b3o) consists of an elongated continuous three-helix bundle, one helix from each monomer, with an overall length of the central stalk plus the base of 190 Å (Fig. S2b) (40). At the tip of the extended central helices, the FPs are located for insertion into the host membrane. In the pre-fusion cryo-EM structure (3jcl), the helix is broken at the middle into two helices, folded back to resemble a 'loaded spring' with an overall stalk length of 85 Å (Fig. S2a) (59). In the pre-fusion state, the FPs are located away from the host membrane (Fig. S2a). Therefore, the length of fusion-active intermediate(s) is at least twice that in the pre-fusion state, which should be sufficient to place the FPs of the S protein near the host cellular membrane.

In order to understand the conversion mechanism from the pre-fusion to the post-fusion state, we are trying to find common structural features between them to identify the moving parts. Since few common features were identified, the conversion must transit through other elusive fusion active intermediates. All fusion-active intermediates share the same extended continuous helices at the 3-fold axis, although they differ greatly in the structures surrounding the central stalk. For example, the extended intermediate has the two membrane-binding motifs of the FP (Fusion Peptide) and TMD (Trans-Membrane Domain) located on the opposite ends of these helices, while in the post-fusion state the two motifs are next to one another after merging the viral and host cellular membranes. The total mass remains unchanged between these structures before no additional proteolysis occurs (Fig. S2). The base of the central stalk in the post-fusion state is much smaller than in the pre-fusion state since residues of the base move to the extended stalk in the post-fusion state (Fig. S2a). The additional C-terminal domain, including the TMD inside the viral membrane, also moves to the tip of the central stalk in the post-fusion state, so that the viral and host membranes are next to one another for eventual merging into a single membrane (Fig. S2b).

The pre-fusion and post-fusion structures both maintain the 3-fold symmetry although they do not share any common 3-fold interactions. At the monomer level there is a superimposable part of a small β-meander of 3 short β-strands plus part of two surrounding helices (Fig. S2i, S2k). However, the orientation of this part of the subunit differs between the two structures relative to the 3-fold axis, which makes alignment of the two structures difficult because each structure can freely slide along the 3-fold axis. For facilitating the comparison, we fixed the Cα of Y1108 to have the same z coordinate along the 3-fold axis in the two structures (Fig. S2i).

An estimated length of the EMD-9597 cryo-EM is about 250 Å at a low-contour level of +4σ, and about 220 Å at a high-contour level of +8σ (Fig. S3a) (59). Regardless of the orientation of this structural feature, we can dock the open-2 conformation of the S trimer (6crz) assuming a

similar structure for the base of the S central stalk, which has been conformed (Fig. S3h) (22, 25). The shape of the extended structural feature fits the central cavity of the S1 trimer (Fig. S3h). Using the common feature of RBD present in both the symmetrized open-2 conformation of the spike trimer and the ACE-2 complex, we docked three ACE-2 dimers onto this structure with the tip of the central stalk located at the middle plane of the host membrane in the super-complex (Fig. 4). The structure has the FPs located at the tip of the central stalk, representing the fusion-active extended intermediate with the FPs ready for insertion into the host membrane.

S3. Productive viral membrane fusion at the cellular level

A productive viral membrane fusion event requires multiple copies of super-complexes of both types. The shortest distance between the membranes of the virus and the host cell occurs when the S trimer binds three ACE-2 dimers at the 3-fold axis of the S trimer at the midpoint of the super-complexes (Fig. 4). Having three ACE-2 dimers per spike trimer holding the host membrane in a tripodal configuration, ensures that the extended S2 central stalk inserts its FP into the host membrane. If the S2 central stalk is extended without tripodal support, such as binding one ACE-2 dimer to a single RBD of the S trimer, there is no guarantee that the FP of the extended S2 central stalk will be inserted into the host cellular membrane. In fact, when the PD (Peptidase Domain) of the ACE-2 dimer adopts an open conformation, the viral membrane and the host cellular membrane are in an angle of 17° and the shortest distance is no longer at the 3-fold axis of the S trimer at the midpoint of the super-complexes (Fig. 3). The distance between the two membranes is gradually shortened and becomes the shortest in the fully closed conformation of the ACE-2 dimers when the PD of ACE-2 dimer undergoes an open-to-closed transition. Therefore, the fusion-active trimeric spike protein requires not only that it binds three ACE-2 dimers, but also that ACE-2 is in an inactive closed conformation.

Given the orientation of the S2 central stalk in a hemi-fusion state is parallel to the both viral and host cellular membranes (29, 30), the formation of three spike trimers in the hemi-fusion state can create a triangle-like pore connecting the two membrane with an edge length of ~ 190 Å, a pore large enough for the genetic materials of SARS-CoV-2 to enter the host cell. When the number of spike trimers is fewer than three copies, such a pore would be difficult to create or to maintain. Therefore, the productive membrane fusion may require at least three spike trimers plus six to nine ACE-2 dimers for their cooperativity. When a host cell does not have a sufficient number of ACE-2 dimers, the tethered SARS-CoV-2 to the cell remains non-invasive with no membrane fusion. In misfiring of unproductive conversion of the S2 trimer from the pre-fusion to post-fusion states without being near the host cellular membrane, both FP and TMD are next to each other inside the own viral membrane as observed *in situ* imaging (16, 17, 67). This post-fusion S2 trimer is incapable for the productive viral membrane fusion reaction.

A recent study based on single-molecule fluorescence spectroscopy has determined the stoichiometry of receptor to spike trimer for the fusion-active complex of HIV-1 gp120 trimer to solubilized T-cell CD4 receptor (68). In HIV-1, the S trimer is similar to the gp160 trimer, which is cleaved by furin to result in gp120 and gp41 trimers, equivalent to S1 and S2 trimers of SARS-CoV-2, respectively. An initial binding involves one receptor per gp120 trimer. One often sees a significant fraction of the three receptors per gp120 trimer with an increasing ratio of receptor to the gp120 trimer to a sufficiently high value. Only a small fraction of an intermediate state containing two receptors per gp120 trimer due to a very strong negative cooperativity for binding the second receptor but a strong positive cooperativity for the third receptor (68). The presence of three CD4 receptor per gp120 has been independently confirmed by another study (69). This cooperativity likely prevents spike trimers from misfiring the ‘loaded spring’ when fewer than three receptors are bound. Similarly, the productive pre-fusion to post-fusion conversion of

hemagglutinin (spike) trimer of H. influenza virus is also known to require the binding of three receptors per hemagglutinin trimer (70).

Our computational modeling provides a new direction in understanding the viral membrane fusion process. Recently, Kwong and colleagues examined cryo-EM structures, thermodynamic properties, and the protonation state of D614 side chain and its variance D614G at pH 7.4 and pH 4.0 combined with molecular dynamic simulations of trimeric spike protein (71). Their results provide an explanation why this mutant is more infectious than the wildtype D614 version (72). This mutation may have altered the dynamic properties of trimeric spike protein by stabilizing its open conformation in binding ACE-2 dimers during the viral membrane fusion process (73).

S4. Inactivation of peptidase activity of ACE-2 upon binding S trimers of SARS-CoV-2

An initial clinical study reported that about 15% of COVID-19 patients suffered from hypertension although the actual percentage has been disputed (74-78). In other studies, the percentage of COVID-19 patients with hypertension was lower than other patients infected with different viruses or the general population (75-78). We show that the initial binding of SARS-CoV-2 may lead to inactivation of ACE-2 enzymatic activity due to geometric constraints at the cellular level, establishing a relationship between SARS-CoV-2 and ACE-2 inactivation. Binding SARS-CoV-2 to ACE-2 could inactivate the ACE-2 function, essentially resulting in a loss-of-function phenotype of ACE-2. This explains how SARS-CoV-2 infection would predominately perturb the renin-angiotensin (ACE/ACE-2) system and energy metabolism (79). As a consequence, the death of COVID-19 patients is often associated with multiple organ failure. In general, elderly men suffering from diabetes or high blood pressure are often very susceptible to SARS-CoV-2 infection and have a high mortality rate. Their morbidity and mortality are correlated with an increased overall cellular level of ACE-2 in vital organs whereas children and women are often resistant to the virus and have a much higher recovery rate (60, 80-82). SARS-CoV-2 infection is limited to the mucous membrane of the respiratory tract of children and women, but not in vital organs where the overall cellular ACE-2 levels are often very low. These locally infected viruses are eventually cleared from the respiratory tract and the patients recover. Given the important role of human ACE-2 in the production of the vasodilator 7-residue peptide hormone angiotensin (residues 1-7) for vascular remodeling (83, 84), ACE-2 and angiotensin (residues 1-7) are essential for protection of many vital organs (85-88). In the case of insufficient cellular ACE-2, the recombinant human ACE-2 can be used as a supplement for organ protection (85-88).

It has been proposed that the recombinant human extracellular ACE-2 (rhACE-2) domains in its soluble form could be used as treatment for COVID-19 patients (63, 64). Binding rhACE-2 to SARS-CoV-2 not only can prevent attachment to the host cellular membrane, but also may prematurely trigger the large conformational changes of the S2 central stalk, causing misfiring of the one-time-only S2 fusion capacity. Treatment of a cohort of COVID-19 patients with the rhACE-2 is currently underway in China (63, 64). We propose that it might be more beneficial to use the peptidase domain-only of the recombinant human ACE-2 for treatment of COVID-19 patients. This domain may remain active for processing angiotensin-2 to angiotensin (residues 1-7) even after it binds the S protein of SARS-CoV-2.

Video titles

Video 1A. View of closed spike trimer with all three RBDs in the "down" position.
Video 1B. Comparison of the spike trimers between three "down" RBDs and one two "down"/one "up" RBDs.

Video 1C. Symmetrized opening and closing of the central pore of the spike trimer with "up" and "down" motions of the RBDs.

Video 2A. The opening and closing motion of the ACE2 active site cleft with and within an inhibitor in complex with the RBDs.
Video 2B. The same as video 2A but with the two spiker trimers.

Video 3A. Motions of the RBDs from open1 to open2 positions in complex with three ACE2 dimers.
Video 3B. View of a super-complex of four spike trimers with three ACE2 dimers
Video 3C. View of a super-complex of one spike trimer in the post-fusion state with three ACE2 dimers.

Supporting Figures

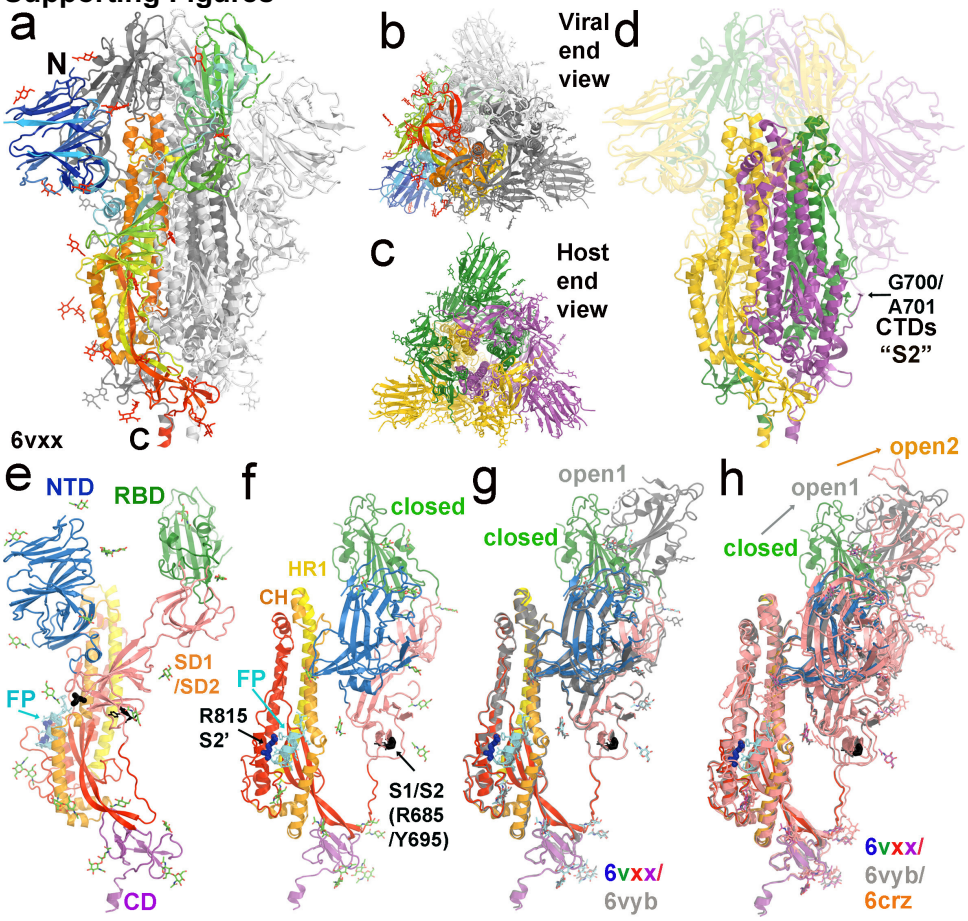

Fig. S1. Trimeric spike structure in a pre-fusion state. (a) One monomer is colored in blue-to-red rainbow from the N-to-C sequence, and two other monomers in grey and silver surfaces. Viral membrane is located at the bottom, and host membrane is located at the top. (b) Viewed from viral membrane end. (c) Viewed from host membrane end. (d) The S1 fragment (after cleavage S1/S2 sites at R685/Y595) are in transparency mode, and the three S2 fragments form the trimer core, which we chose the G700/A701 as a junction, instead of the canonic S2 cleavage site at Y595 because structurally the remaining 100 residues of S2 are more tightly associated with the S1 fragment, which is considered part of S1 and is not involved in the S2 refolding during viral membrane fusion. (e, f) Two orthogonal views of monomer architecture: NTD (blue), SD1/SD2 (salmon), RBD (forest green), unnamed S2 fragment core (red), FP (cyan), HR1 (yellow), CH (brown), and CD (magenta), and the S1/S2, and S2' site (black). R815 at the S2' site and residues

near R685 at the S1 site (missing in the model) and at Y695 are also in black. FP is in cyan stick model. (g) Superposition of the closed 6vxx conformation (multicolor) with the 6vyb open-1 conformation (grey). (h Superposition of the closed 6vxx, 6vyb open-1, and 6crz open-2 (salmon) conformations

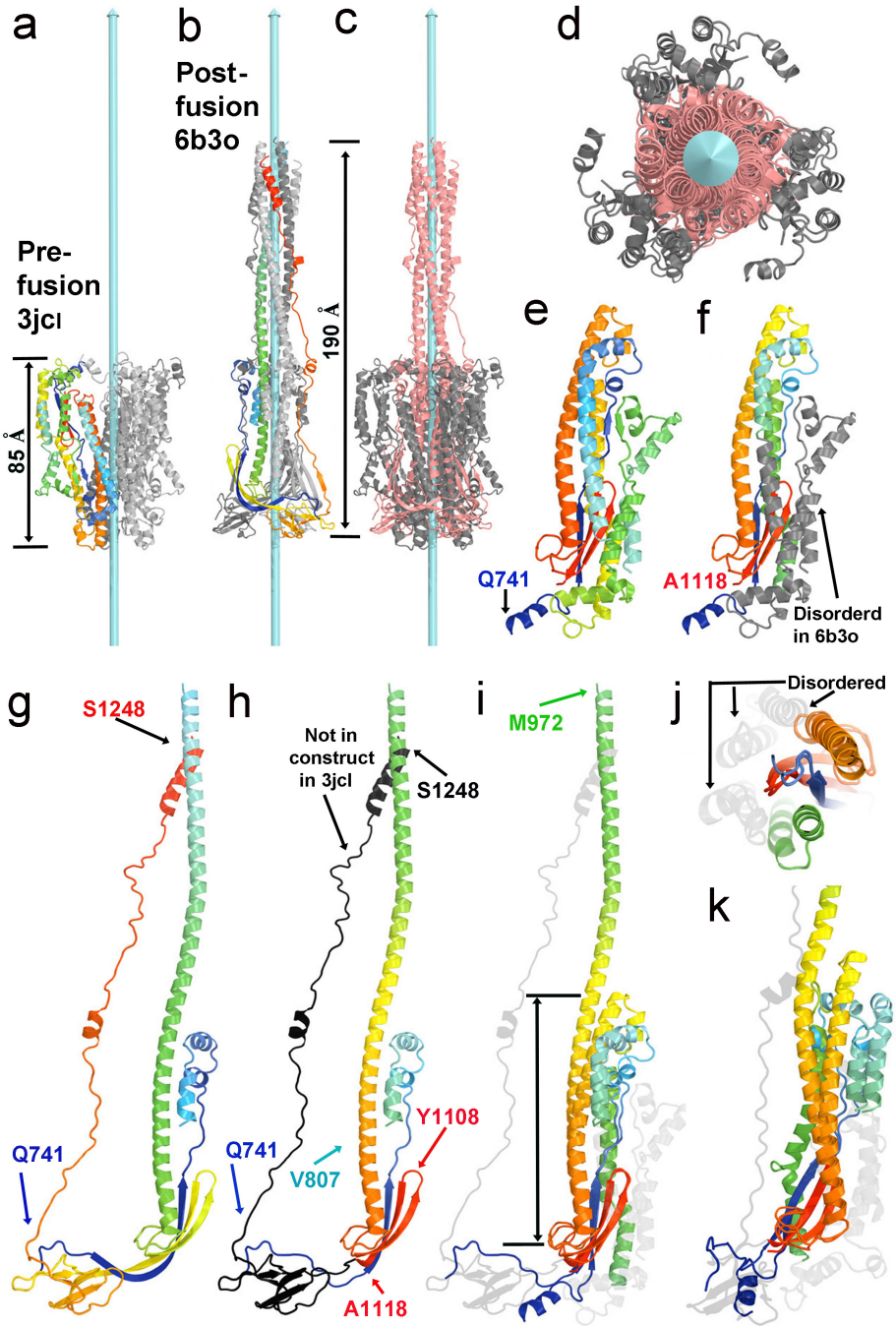

Fig. S2. The refolding of the central stalk of S2 subunit. (a) The pre-fusion state (3jcl) of MHV S2 with helices folded back as in a loaded spring, having an approximate stalk length of about 85 Å. One monomer is rainbow colored from N-to-C termini, and the other two are in grey and silver. (b) The post-fusion (6b3o) of MHV S2 with central helices extended in a released spring, having an approximate length of about 190 Å. (c, d) Two orthogonal views of superposition of the pre-fusion (grey) and post-fusion (salmon) states by aligning the Y1108 Cα with the position projected

on the 3-fold axis. Aside from the 2-fold symmetry, there is no common point for aligning the two trimers. In monomer, a small β-meander of three short β-strands plus part of one helix have the same folding in the two structures, but the relationship to the 3-fold axis between the two structures is unrelated. (e, f) S2 monomer in the pre-fusion state with the residues in grey that are present in the protein but disordered in this structure. (g, h) S2 monomer in the post-fusion state in rainbow with the residues in black that are not present in the 3jcl construct but are ordered in this structure (3b3o). (i-k) Three views of superposition of these two structures using β-meander with part of α-helix. (i) Standard view. Double-headed arrow indicates the parts that are superimposable. (j) Close-up view down the β-meander. (k) Close-up view of the stalk base with superimposable parts indicated with double-headed arrow in (i).

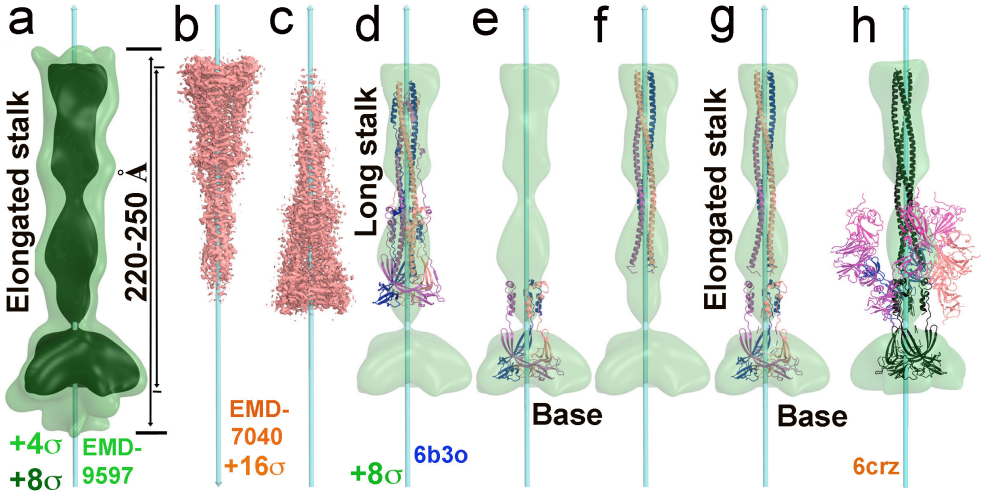

Fig. S3. A piecewise assembly of fusion-active extended intermediate of the S2 central stalk. (a) EMD-9597 map contoured at +4σ (light green) and +8σ (dark green) with estimated length of the SARS-CoV S2 stalk of 220 Å and 250 Å at these two contouring levels, respectively. (b) A reference EMD-7040 map for the post-fusion structure of the MHV S3 stalk in one interpretation n which over one-third of the stalk length and over one-third to half of the volumetric data remain unexplained. (c) New orientation of the stalk. (D-G) Fitting of the 3b3o model derived from EMD-7040 into the EMD-9597 map. (d) Initial fitting as a single rigid body. (e) Fitting of the stalk base as a single rigid body. (f) Fitting of three central helices of the stalk as a single rigid body. (g) Sum view of the two-body rigid-body fitted structures. (h) Docking S1 trimer in open2-conformation (6crz) using the common feature of the stalk base structure.

Additional Supporting References

1. Zhou P, Yang XL, Wang XG, Hu B, Zhang L, Zhang W, Si HR, Zhu Y, Li B, Huang CL, Chen HD, Chen J, Luo Y, Guo H, Jiang RD, Liu MQ, Chen Y, Shen XR, Wang X, Zheng XS, Zhao K, Chen QJ, Deng F, Liu LL, Yan B, Zhan FX, Wang YY, Xiao GF, Shi ZL. 2020. A pneumonia outbreak associated with a new coronavirus of probable bat origin. Nature 579:270-273.
2. Wu F, Zhao S, Yu B, Chen YM, Wang W, Song ZG, Hu Y, Tao ZW, Tian JH, Pei YY, Yuan ML, Zhang YL, Dai FH, Liu Y, Wang QM, Zheng JJ, Xu L, Holmes EC, Zhang YZ. 2020. A new coronavirus associated with human respiratory disease in China. Nature 579:265-269.
3. Lu R, Zhao X, Li J, Niu P, Yang B, Wu H, Wang W, Song H, Huang B, Zhu N, Bi Y, Ma X, Zhan F, Wang L, Hu T, Zhou H, Hu Z, Zhou W, Zhao L, Chen J, Meng Y, Wang J, Lin Y,

Yuan J, Xie Z, Ma J, Liu WJ, Wang D, Xu W, Holmes EC, Gao GF, Wu G, Chen W, Shi W, Tan W. 2020. Genomic characterisation and epidemiology of 2019 novel coronavirus: implications for virus origins and receptor binding. Lancet 395:565-574.

4. Zhu N, Zhang D, Wang W, Li X, Yang B, Song J, Zhao X, Huang B, Shi W, Lu R, Niu P, Zhan F, Ma X, Wang D, Xu W, Wu G, Gao GF, Tan W, China Novel Coronavirus I, Research T. 2020. A Novel Coronavirus from Patients with Pneumonia in China, 2019. N Engl J Med 382:727-733.
5. Lan J, Ge J, Yu J, Shan S, Zhou H, Fan S, Zhang Q, Shi X, Wang Q, Zhang L, Wang X. 2020. Structure of the SARS-CoV-2 spike receptor-binding domain bound to the ACE2 receptor. Nature 581:215-220.
6. Shang J, Ye G, Shi K, Wan Y, Luo C, Aihara H, Geng Q, Auerbach A, Li F. 2020. Structural basis of receptor recognition by SARS-CoV-2. Nature 581:221-224.
7. Yan R, Zhang Y, Li Y, Xia L, Guo Y, Zhou Q. 2020. Structural basis for the recognition of SARS-CoV-2 by full-length human ACE2. Science 367:1444-1448.
8. Cao Y, Su B, Guo X, Sun W, Deng Y, Bao L, Zhu Q, Zhang X, Zheng Y, Geng C, Chai X, He R, Li X, Lv Q, Zhu H, Deng W, Xu Y, Wang Y, Qiao L, Tan Y, Song L, Wang G, Du X, Gao N, Liu J, Xiao J, Su XD, Du Z, Feng Y, Qin C, Qin C, Jin R, Xie XS. 2020. Potent neutralizing antibodies against SARS-CoV-2 identified by high-throughput single-cell sequencing of convalescent patients' B cells. Cell doi:10.1016/j.cell.2020.05.025.
9. Barnes CO, West AP, Jr., Huey-Tubman KE, Hoffmann MAG, Sharaf NG, Hoffman PR, Koranda N, Gristick HB, Gaebler C, Muecksch F, Lorenzi JCC, Finkin S, Hagglof T, Hurley A, Millard KG, Weisblum Y, Schmidt F, Hatziioannou T, Bieniasz PD, Caskey M, Robbiani DF, Nussenzweig MC, Bjorkman PJ. 2020. Structures of Human Antibodies Bound to SARS-CoV-2 Spike Reveal Common Epitopes and Recurrent Features of Antibodies. Cell 182:828-842 e16.
10. Xia S, Liu M, Wang C, Xu W, Lan Q, Feng S, Qi F, Bao L, Du L, Liu S, Qin C, Sun F, Shi Z, Zhu Y, Jiang S, Lu L. 2020. Inhibition of SARS-CoV-2 (previously 2019-nCoV) infection by a highly potent pan-coronavirus fusion inhibitor targeting its spike protein that harbors a high capacity to mediate membrane fusion. Cell Res 30:343-355.
11. Tang T, Bidon M, Jaimes JA, Whittaker GR, Daniel S. 2020. Coronavirus membrane fusion mechanism offers a potential target for antiviral development. Antiviral Res 178:104792.
12. Ng ML, Lee JW, Leong ML, Ling AE, Tan HC, Ooi EE. 2004. Topographic changes in SARS coronavirus-infected cells at late stages of infection. Emerg Infect Dis 10:1907-14.
13. Neuman BW, Adair BD, Yoshioka C, Quispe JD, Orca G, Kuhn P, Milligan RA, Yeager M, Buchmeier MJ. 2006. Supramolecular architecture of severe acute respiratory syndrome coronavirus revealed by electron cryomicroscopy. J Virol 80:7918-28.
14. Barcena M, Oostergetel GT, Bartelink W, Faas FG, Verkleij A, Rottier PJ, Koster AJ, Bosch BJ. 2009. Cryo-electron tomography of mouse hepatitis virus: Insights into the structure of the coronavirion. Proc Natl Acad Sci U S A 106:582-7.
15. Ertel KJ, Benefield D, Castano-Diez D, Pennington JG, Horswill M, den Boon JA, Otegui MS, Ahlquist P. 2017. Cryo-electron tomography reveals novel features of a viral RNA replication compartment. Elife 6.
16. Klein S, Cortese M, Winter SL, Wachsmuth-Melm M, Neufeldt CJ, Cerikan B, Stanifer ML, Boulant S, Bartenschlager R, Chlanda P. 2020. SARS-CoV-2 structure and

replicaiton characrterized by in situ cryo-electron tomography. bioRxiv preprint: doi: https://doiorg/101101/20200623167064:Unpublished.
17. Turonova B, Sikora M, Schurmann C, Hagen WJH, Welsch S, Blanc FEC, von Bulow S, Gecht M, Bagola K, Horner C, van Zandbergen G, Landry J, de Azevedo NTD, Mosalaganti S, Schwarz A, Covino R, Muhlebach MD, Hummer G, Krijnse Locker J, Beck M. 2020. In situ structural analysis of SARS-CoV-2 spike reveals flexibility mediated by three hinges. Science doi:10.1126/science.abd5223.
18. Ke Z, Oton J, Qu K, Cortese M, Zila V, McKeane L, Nakane T, Zivanov J, Neufeldt CJ, Cerikan B, Lu JM, Peukes J, Xiong X, Krausslich HG, Scheres SHW, Bartenschlager R, Briggs JAG. 2020. Structures and distributions of SARS-CoV-2 spike proteins on intact virions. Nature doi:10.1038/s41586-020-2665-2.
19. Wrapp D, Wang N, Corbett KS, Goldsmith JA, Hsieh CL, Abiona O, Graham BS, McLellan JS. 2020. Cryo-EM structure of the 2019-nCoV spike in the prefusion conformation. Science 367:1260-1263.
20. Walls AC, Park YJ, Tortorici MA, Wall A, McGuire AT, Veesler D. 2020. Structure, Function, and Antigenicity of the SARS-CoV-2 Spike Glycoprotein. Cell 181:281-292 e6.
21. Li F. 2016. Structure, Function, and Evolution of Coronavirus Spike Proteins. Annu Rev Virol 3:237-261.
22. Song W, Gui M, Wang X, Xiang Y. 2018. Cryo-EM structure of the SARS coronavirus spike glycoprotein in complex with its host cell receptor ACE2. PLoS Pathog 14:e1007236.
23. Yuan Y, Cao D, Zhang Y, Ma J, Qi J, Wang Q, Lu G, Wu Y, Yan J, Shi Y, Zhang X, Gao GF. 2017. Cryo-EM structures of MERS-CoV and SARS-CoV spike glycoproteins reveal the dynamic receptor binding domains. Nat Commun 8:15092.
24. Gui M, Song W, Zhou H, Xu J, Chen S, Xiang Y, Wang X. 2017. Cryo-electron microscopy structures of the SARS-CoV spike glycoprotein reveal a prerequisite conformational state for receptor binding. Cell Res 27:119-129.
25. Kirchdoerfer RN, Wang N, Pallesen J, Wrapp D, Turner HL, Cottrell CA, Corbett KS, Graham BS, McLellan JS, Ward AB. 2018. Stabilized coronavirus spikes are resistant to conformational changes induced by receptor recognition or proteolysis. Sci Rep 8:15701.
26. Li F, Li W, Farzan M, Harrison SC. 2005. Structure of SARS coronavirus spike receptor-binding domain complexed with receptor. Science 309:1864-8.
27. Tipnis SR, Hooper NM, Hyde R, Karran E, Christie G, Turner AJ. 2000. A human homolog of angiotensin-converting enzyme. Cloning and functional expression as a captopril-insensitive carboxypeptidase. J Biol Chem 275:33238-43.
28. Donoghue M, Hsieh F, Baronas E, Godbout K, Gosselin M, Stagliano N, Donovan M, Woolf B, Robison K, Jeyaseelan R, Breitbart RE, Acton S. 2000. A novel angiotensin-converting enzyme-related carboxypeptidase (ACE2) converts angiotensin I to angiotensin 1-9. Circ Res 87:E1-9.
29. Harrison SC. 2005. Mechanism of membrane fusion by viral envelope proteins. Adv Virus Res 64:231-61.
30. Harrison SC. 2008. Viral membrane fusion. Nat Struct Mol Biol 15:690-8.
31. Harrison SC. 2015. Viral membrane fusion. Virology 479-480:498-507.

32. White JM, Delos SE, Brecher M, Schornberg K. 2008. Structures and mechanisms of viral membrane fusion proteins: multiple variations on a common theme. Crit Rev Biochem Mol Biol 43:189-219.
33. Kielian M. 2014. Mechanisms of Virus Membrane Fusion Proteins. Annu Rev Virol 1:171-89.
34. Rey FA, Lok SM. 2018. Common Features of Enveloped Viruses and Implications for Immunogen Design for Next-Generation Vaccines. Cell 172:1319-1334.
35. Colman PM, Lawrence MC. 2003. The structural biology of type I viral membrane fusion. Nat Rev Mol Cell Biol 4:309-19.
36. Cai Y, Zhang J, Xiao T, Peng H, Sterling SM, Walsh RM, Jr., Rawson S, Rits-Volloch S, Chen B. 2020. Distinct conformational states of SARS-CoV-2 spike protein. Science doi:10.1126/science.abd4251.
37. Pancera M, Zhou T, Druz A, Georgiev IS, Soto C, Gorman J, Huang J, Acharya P, Chuang GY, Ofek G, Stewart-Jones GB, Stuckey J, Bailer RT, Joyce MG, Louder MK, Tumba N, Yang Y, Zhang B, Cohen MS, Haynes BF, Mascola JR, Morris L, Munro JB, Blanchard SC, Mothes W, Connors M, Kwong PD. 2014. Structure and immune recognition of trimeric pre-fusion HIV-1 Env. Nature 514:455-61.
38. Schaffer L. 1994. A model for insulin binding to the insulin receptor. Eur J Biochem 221:1127-32.
39. Li J, Choi E, Yu H, Bai XC. 2019. Structural basis of the activation of type 1 insulin-like growth factor receptor. Nat Commun 10:4567.
40. Uchikawa E, Choi E, Shang G, Yu H, Bai XC. 2019. Activation mechanism of the insulin receptor revealed by cryo-EM structure of the fully liganded receptor-ligand complex. Elife 8.
41. Sainz B, Jr., Rausch JM, Gallaher WR, Garry RF, Wimley WC. 2005. The aromatic domain of the coronavirus class I viral fusion protein induces membrane permeabilization: putative role during viral entry. Biochemistry 44:947-58.
42. Guillen J, Kinnunen PK, Villalain J. 2008. Membrane insertion of the three main membranotropic sequences from SARS-CoV S2 glycoprotein. Biochim Biophys Acta 1778:2765-74.
43. Mahajan M, Bhattacharjya S. 2015. NMR structures and localization of the potential fusion peptides and the pre-transmembrane region of SARS-CoV: Implications in membrane fusion. Biochim Biophys Acta 1848:721-30.
44. Mahajan M, Chatterjee D, Bhuvaneswari K, Pillay S, Bhattacharjya S. 2018. NMR structure and localization of a large fragment of the SARS-CoV fusion protein: Implications in viral cell fusion. Biochim Biophys Acta Biomembr 1860:407-415.
45. Meher G, Bhattacharjya S, Chakraborty H. 2019. Membrane Cholesterol Modulates Oligomeric Status and Peptide-Membrane Interaction of Severe Acute Respiratory Syndrome Coronavirus Fusion Peptide. J Phys Chem B 123:10654-10662.
46. Chakraborty H, Bhattacharjya S. 2020. Mechanistic insights of host cell fusion of SARS-CoV-1 and SARS-CoV-2 from atomic resolution structure and membrane dynamics. Biophys Chem 265:106438.
47. Pattnaik GP, Bhattacharjya S, Chakraborty H. 2021. Enhanced Cholesterol-Dependent Hemifusion by Internal Fusion Peptide 1 of SARS Coronavirus-2 Compared to Its N-Terminal Counterpart. Biochemistry 60:559-562.

48. Borkotoky S, Dey D, Banerjee M. 2021. Computational Insight Into the Mechanism of SARS-CoV-2 Membrane Fusion. J Chem Inf Model 61:423-431.
49. Lutkenhaus J, Addinall SG. 1997. Bacterial cell division and the Z ring. Annu Rev Biochem 66:93-116.
50. Miller AL. 2011. The contractile ring. Curr Biol 21:R976-8.
51. Emsley P, Cowtan K. 2004. Coot: model-building tools for molecular graphics. Acta Crystallogr D Biol Crystallogr 60:2126-32.
52. Winn MD, Ballard CC, Cowtan KD, Dodson EJ, Emsley P, Evans PR, Keegan RM, Krissinel EB, Leslie AG, McCoy A, McNicholas SJ, Murshudov GN, Pannu NS, Potterton EA, Powell HR, Read RJ, Vagin A, Wilson KS. 2011. Overview of the CCP4 suite and current developments. Acta Crystallogr D Biol Crystallogr 67:235-42.
53. Delano WL. 2009. The Pymol Molecular Graphics System. Delano Scientific, San Carlos, CA.
54. Jo S, Vargyas M, Vasko-Szedlar J, Roux B, Im W. 2008. PBEQ-Solver for online visualization of electrostatic potential of biomolecules. Nucleic Acids Res 36:W270-5.
55. Woo H, Park SJ, Choi YK, Park T, Tanveer M, Cao Y, Kern NR, Lee J, Yeom MS, Croll TI, Seok C, Im W. 2020. Developing a Fully-glycosylated Full-length SARS-CoV-2 Spike Protein Model in a Viral Membrane. J Phys Chem B doi:10.1021/acs.jpcb.0c04553.
56. Sztain T, Ahn SH, Bogetti AT, Casalino L, Goldsmith JA, McCool RS, Kearns FL, McCammon JA, McLellan JS, Chong LT, Amaro RE. 2021. A glycan gate controls opening of the SARS-CoV-2 spike protein. bioRxiv doi:10.1101/2021.02.15.431212.
57. Guo L, Bi W, Wang X, Xu W, Yan R, Zhang Y, Zhao K, Li Y, Zhang M, Cai X, Jiang S, Xie Y, Zhou Q, Lu L, Dang B. 2021. Engineered trimeric ACE2 binds viral spike protein and locks it in "Three-up" conformation to potently inhibit SARS-CoV-2 infection. Cell Res 31:98-100.
58. Towler P, Staker B, Prasad SG, Menon S, Tang J, Parsons T, Ryan D, Fisher M, Williams D, Dales NA, Patane MA, Pantoliano MW. 2004. ACE2 X-ray structures reveal a large hinge-bending motion important for inhibitor binding and catalysis. J Biol Chem 279:17996-8007.
59. Walls AC, Tortorici MA, Snijder J, Xiong X, Bosch BJ, Rey FA, Veesler D. 2017. Tectonic conformational changes of a coronavirus spike glycoprotein promote membrane fusion. Proc Natl Acad Sci U S A 114:11157-11162.
60. Verdecchia P, Cavallini C, Spanevello A, Angeli F. 2020. The pivotal link between ACE2 deficiency and SARS-CoV-2 infection. Eur J Intern Med 76:14-20.
61. Kuba K, Imai Y, Rao S, Gao H, Guo F, Guan B, Huan Y, Yang P, Zhang Y, Deng W, Bao L, Zhang B, Liu G, Wang Z, Chappell M, Liu Y, Zheng D, Leibbrandt A, Wada T, Slutsky AS, Liu D, Qin C, Jiang C, Penninger JM. 2005. A crucial role of angiotensin converting enzyme 2 (ACE2) in SARS coronavirus-induced lung injury. Nat Med 11:875-9.
62. Imai Y, Kuba K, Rao S, Huan Y, Guo F, Guan B, Yang P, Sarao R, Wada T, Leong-Poi H, Crackower MA, Fukamizu A, Hui CC, Hein L, Uhlig S, Slutsky AS, Jiang C, Penninger JM. 2005. Angiotensin-converting enzyme 2 protects from severe acute lung failure. Nature 436:112-6.
63. Wang K, Gheblawi M, Oudit GY. 2020. Angiotensin Converting Enzyme 2: A Double-Edged Sword. Circulation In Press.
64. Batlle D, Wysocki J, Satchell K. 2020. Soluble angiotensin-converting enzyme 2: a potential approach for coronavirus infection therapy? Clin Sci (Lond) 134:543-545.

65. Kirchdoerfer RN, Ward AB. 2019. Structure of the SARS-CoV nsp12 polymerase bound to nsp7 and nsp8 co-factors. Nat Commun 10:2342.
66. Fan X, Cao D, Kong L, Zhang X. 2020. Cryo-EM structure of SARS-CoV spike glycoprotein in post-fusion state. http://wwwchinaxivorg/user/downloadhtm?id=30394:Unpublished.
67. Liu C, Yang Y, Gao Y, Shen C, Ju B, Liu C, Tang X, Wei J, Ma X, Liu W, Xu S, Liu Y, Yuan J, Wu J, Liu Z, Zhang Z, Wang P, Liu L. 2020. Viral architecture of SARS-CoV-2 with post-fusion spike revealed by cryo-EM. BioRxiV preprint: doi: https://doiorg/101101/20200302972927:Unpublished.
68. Agrawal P, DeVico AL, Foulke JS, Jr., Lewis GK, Pazgier M, Ray K. 2019. Stoichiometric Analyses of Soluble CD4 to Native-like HIV-1 Envelope by Single-Molecule Fluorescence Spectroscopy. Cell Rep 29:176-186 e4.
69. Ma X, Lu M, Gorman J, Terry DS, Hong X, Zhou Z, Zhao H, Altman RB, Arthos J, Blanchard SC, Kwong PD, Munro JB, Mothes W. 2018. HIV-1 Env trimer opens through an asymmetric intermediate in which individual protomers adopt distinct conformations. Elife 7.
70. Weis W, Brown JH, Cusack S, Paulson JC, Skehel JJ, Wiley DC. 1988. Structure of the influenza virus haemagglutinin complexed with its receptor, sialic acid. Nature 333:426-31.
71. Zhou T, Tsybovsky Y, Olia AS, Gorman J, Rapp MA, Cerutti G, Katsamba PS, Nazzari A, Schon A, Wang PD, Bimela J, Shi W, Teng IT, Zhang B, Boyington JC, Chuang GY, Sampson JM, Sastry M, Stephens T, Stuckey J, Wang S, Friesner RA, Ho DD, Mascola JR, Shapiro L, Kwong PD. 2020. A pH-dependent switch mediates conformational masking of SARS-CoV-2 spike. bioRxiv doi:10.1101/2020.07.04.187989.
72. Korber B, Fischer WM, Gnanakaran S, Yoon H, Theiler J, Abfalterer W, Hengartner N, Giorgi EE, Bhattacharya T, Foley B, Hastie KM, Parker MD, Partridge DG, Evans CM, Freeman TM, de Silva TI, Sheffield C-GG, McDanal C, Perez LG, Tang H, Moon-Walker A, Whelan SP, LaBranche CC, Saphire EO, Montefiori DC. 2020. Tracking Changes in SARS-CoV-2 Spike: Evidence that D614G Increases Infectivity of the COVID-19 Virus. Cell 182:812-827 e19.
73. Mansbach RA, Chakraborty S, Nguyen K, Montefiori D, Korber B, Gnanakaran S. 2020. The SARS-CoV-2 Spike Variant D614G Favors an Open Conformational State. bioRxiv doi:10.1101/2020.07.26.219741.
74. Vaduganathan M, Solomon SD. 2020. Renin-Angiotensin-Aldosterone System Inhibitors in Covid-19. Reply. N Engl J Med 382:e92.
75. Fang L, Karakiulakis G, Roth M. 2020. Are patients with hypertension and diabetes mellitus at increased risk for COVID-19 infection? Lancet Respir Med 8:e21.
76. Esler M, Esler D. 2020. Can angiotensin receptor-blocking drugs perhaps be harmful in the COVID-19 pandemic? J Hypertens 38:781-782.
77. Sommerstein R, Kochen MM, Messerli FH, Grani C. 2020. Coronavirus Disease 2019 (COVID-19): Do Angiotensin-Converting Enzyme Inhibitors/Angiotensin Receptor Blockers Have a Biphasic Effect? J Am Heart Assoc 9:e016509.
78. Diaz JH. 2020. Hypothesis: angiotensin-converting enzyme inhibitors and angiotensin receptor blockers may increase the risk of severe COVID-19. J Travel Med 27.
79. Ghosh A, Vishveshwara S. 2008. Variations in Clique and Community Patterns in Protein Structures during Allosteric Communication: Investigation of Dynamically

Equilibrated Structures of Methionyl tRNA Synthetase Complexes. Biochemistry 47:11398-11407.
80. Ciaglia E, Vecchione C, Puca AA. 2020. COVID-19 Infection and Circulating ACE2 Levels: Protective Role in Women and Children. Front Pediatr 8:206.
81. Patel AB, Verma A. 2020. Nasal ACE2 Levels and COVID-19 in Children. JAMA doi:10.1001/jama.2020.8946.
82. Sama IE, Ravera A, Santema BT, van Goor H, Ter Maaten JM, Cleland JGF, Rienstra M, Friedrich AW, Samani NJ, Ng LL, Dickstein K, Lang CC, Filippatos G, Anker SD, Ponikowski P, Metra M, van Veldhuisen DJ, Voors AA. 2020. Circulating plasma concentrations of angiotensin-converting enzyme 2 in men and women with heart failure and effects of renin-angiotensin-aldosterone inhibitors. Eur Heart J 41:1810-1817.
83. Zhang Z, Chen L, Zhong J, Gao P, Oudit GY. 2014. ACE2/Ang-(1-7) signaling and vascular remodeling. Sci China Life Sci 57:802-8.
84. Patel VB, Zhong JC, Fan D, Basu R, Morton JS, Parajuli N, McMurtry MS, Davidge ST, Kassiri Z, Oudit GY. 2014. Angiotensin-converting enzyme 2 is a critical determinant of angiotensin II-induced loss of vascular smooth muscle cells and adverse vascular remodeling. Hypertension 64:157-64.
85. Oudit GY, Penninger JM. 2011. Recombinant human angiotensin-converting enzyme 2 as a new renin-angiotensin system peptidase for heart failure therapy. Curr Heart Fail Rep 8:176-83.
86. Patel VB, Lezutekong JN, Chen X, Oudit GY. 2017. Recombinant Human ACE2 and the Angiotensin 1-7 Axis as Potential New Therapies for Heart Failure. Can J Cardiol 33:943-946.
87. Patel VB, Zhong JC, Grant MB, Oudit GY. 2016. Role of the ACE2/Angiotensin 1-7 Axis of the Renin-Angiotensin System in Heart Failure. Circ Res 118:1313-26.
88. Gheblawi M, Wang K, Viveiros A, Nguyen Q, Zhong JC, Turner AJ, Raizada MK, Grant MB, Oudit GY. 2020. Angiotensin-Converting Enzyme 2: SARS-CoV-2 Receptor and Regulator of the Renin-Angiotensin System: Celebrating the 20th Anniversary of the Discovery of ACE2. Circ Res 126:1456-1474.